Thermodynamic consistency of liquid-gas lattice Boltzmann methods: Interfacial property issues

E. S. Kikkinides
Department of Engineering and Management of Energy Resources, University of Western Macedonia, Bakola and Sialvera Street, 50100 Kozani, Greece

A. G. Yiotis, M. E. Kainourgiakis, and A. K. Stubos
Environmental Research Laboratory, National Center for Scientific Research "Demokritos", 15310 Ag. Paraskevi, Athens, Greece
(Received 27 March 2008; revised manuscript received 2 June 2008; published 8 September 2008)

In the present study we examine the thermodynamic consistency of lattice Boltzmann equation (LBE) models that are based on the forcing method by comparing different numerical treatments of the LBE for van der Waals fluids. The different models are applied for the calculation of bulk and interfacial thermodynamic properties at various temperatures. The effect of the interface density gradient parameter, κ, that controls surface tension, is related explicitly with the fluid characteristics, including temperature, molecular diameter, and lattice spacing, through the employment of a proper intermolecular interaction potential. A comprehensive analysis of the interfacial properties reveals some important shortcomings of the LBE methods when central finite difference schemes are employed in the directional derivative calculations and proposes a proper treatment that ensures thermodynamically consistent interfacial properties in accord with the van der Waals theory. The results are found to be in excellent quantitative agreement with exact results of the van der Waals theory preserving all the major features of the interfacial characteristics of vapor-liquid systems of different shapes and sizes.

DOI: 10.1103/PhysRevE.78.036702 PACS number(s): 47.11.−j, 02.70.−c, 05.70.Ce, 68.03.Cd

I. INTRODUCTION

The study of single and multicomponent fluids undergoing phase transitions is a subject of both fundamental and applied scientific research with applications to a wide variety of industrial and environmental processes, including gas and liquid separations and purifications, enhanced oil recovery, underground water pollution, nanotechnology applications, etc. Consequently, any proper treatment of the structure of the liquid-vapor interface and the corresponding surface tension requires a detailed theory for the statistical mechanics of nonuniform fluids [1]. About a century ago, van der Waals introduced a molecular theory for nonpolar fluids utilizing a local Helmholtz free energy density consisting of a uniform term, evaluated at the local mass density, and a nonuniform term that is proportional to the square of the mass density gradient. The above consideration is derived from the expansion of the Helmholtz free energy as a series of density gradients assuming that density is slowly varying throughout the fluid [2–4]. The van der Waals (vdW) model represents even today the simplest molecular model that is qualitatively correct, at least for nonpolar fluids. Over the last three decades, several modified versions have been developed that retain the simplicity of the original theory while yielding much more accurate descriptions of the interfacial fluid properties [5,6]. The vdW model yields explicit expressions for the basic thermodynamic functions and equations for the interfacial density profiles and surface tension of liquid-vapor systems. The assumption of a slowly varying density implies that the system must be close to its critical temperature, although experience has indicated that the validity of the model can be extended to lower temperatures.

Over the years, the continuous development of more rigorous molecular or atomistic models of liquid-vapor systems, in conjunction with the dramatic improvement in computational power, has resulted in a more in-depth understanding of the underlying physics of these systems. Traditional computational fluid dynamics methods have many difficulties and limitations in this area, while molecular simulation models have excessively large computational requirements for the solution of even relatively simple problems, and are limited to extremely small time and/or space scales and simple geometries. In this context, the use of the lattice Boltzmann equation (LBE) method to study multiphase flows has increased significantly over the last decade.

The LBE method is a mesoscopic approach that incorporates microscopic physics at a reasonable computational expense [7–9]. Even though the major focus of the method has been on averaged macroscopic behavior, its kinetic nature can provide many of the advantages of molecular dynamics, bridging the gap between molecular dynamics simulations at the microscopic level and simulations based on macroscopic conservation laws [10]. The LBE method is especially useful for complex systems in which the macroscopic governing equations cannot be determined in a straightforward manner while the microscopic physics is adequately described to a certain level of approximation. Several approaches exist for modeling liquid-vapor fluids using the LBE method. These approaches utilize the basic assumptions of the van der Waals theory and can be classified into two major groups. One approach is based on a free energy formulation of fluid interactions [11–20]. The basic idea behind this approach is to impose an additional constraint on the equilibrium distribution function so that its second moment reproduces the desired pressure tensor, and hence this approach is often called the pressure method. The second approach is guided by an atomistic formalism where interparticle interactions are introduced by the direct inclusion of a forcing term in the LB equation, and hence is called the forcing method [21–31]. Each approach has its own advantages and limitations, nevertheless they both lead to a nonideal vdW equation of state that can produce phase separation.

A major breakthrough in the LBE theory has been the direct derivation of the LB equation from the continuous Boltzmann equation with the Bhatnagar-Gross-Krook (BGK) collision operator [32,33]. The successful establishment of theoretical foundation of the LBE method in the framework of kinetic theory of gases has led to more rigorous ways of incorporating molecular interactions in the LBE following the Bogoliubov-Born-Green-Kirkwood-Yvon (BBGKY) formalism [34–36]. Furthermore, Enskog's extension of Boltzmann's equation for dense gases [37] has been employed in [34,38–41]. In a thermodynamic sense, Boltzmann's equation is applicable only for ideal gases. In order to properly account for the interparticle forces, Enskog's volume exclusion effect terms and intermolecular attraction terms must be included [37].

In their original work, He *et al.* [38] introduced these terms in the form of a forcing term considering interparticle interaction using a mean-field treatment in the same way that the Coulomb interaction among the charged particles of a plasma is treated in Vlasov's equation [38,42]. Later, He and Doolen [34] improved the above model starting from the BBGKY equations and established the thermodynamic foundations of the LBE multiphase models by showing that a kinetic equation that combines Enskog's theory for dense fluids with the mean-field theory for long-range molecular interaction can consistently describe nonideal gases and dense fluid flows. Luo [39,40] carried out a systematic derivation of the lattice Boltzmann equation model for nonideal gases starting from the Enskog equation. The equation of state is obtained and the required thermodynamic consistency is achieved. In all cases the basic features of the vdW theory are retained and these set the thermodynamic limits of the validity of these models.

Based on the approach of He *et al.* [38] and later He and Doolen [34], several LBE models have been proposed using either Lagrangian [43–45] or Eulerian-based finite difference schemes [46–49] for the discretization of the convective (advection) terms. However, the thermodynamic consistency of these models has been disputed [47–50] because most of them fail to provide accurate predictions for the thermodynamic properties, including equilibrium gas and liquid bulk densities, pressure, and chemical potential.

Recently, Wagner [50] has demonstrated that the second-order expansion employed in the LBE models is inadequate for the case of strongly inhomogeneous fluids since it omits non-negligible higher-order terms, which are responsible for obtaining a true equilibrium solution with both a constant chemical potential and a constant pressure. Accordingly, he presented an equilibrium analysis of nonideal lattice Boltzmann methods of sufficient order to identify and include those higher-order terms whose absence leads to a lack of thermodynamic consistency. Moreover, he has argued that a proper numerical expression of the Gibbs-Duhem equation could guarantee that a constant pressure is exactly equivalent to a constant chemical potential, and therefore it would exactly recover equilibrium thermodynamics.

Working along the same line of reasoning, Lee and Lin [51] and later Lee and Fischer [52] have developed LBE models that employ the chemical potential instead of the pressure gradient as the driving force through the Gibbs-Duhem equation. Furthermore, these authors have used alternative numerical schemes for the discretization of the directional derivatives of the LBE model and their results have shown an improved stability and accuracy for large density differences, using a simplified equation of state, during static and dynamic conditions.

Although Wagner's approach [50] fills an important gap in the thermodynamic consistency of LBE models, his in-depth analysis focuses exclusively on the bulk values of gas and liquid density. However, an important issue that remains to be explored in deriving thermodynamically consistent LBE models is the interfacial properties of gas-liquid systems, and more particularly the quantitative description of the interfacial thickness and surface tension of these systems. The Lee and Fischer analysis [52] on the other hand, although looks very promising, has been focusing so far primarily on the reduction of the magnitude of the spurious velocities found in static systems. A thermodynamic analysis on bulk density values and interface properties including surface tension and interface thickness has been limited on a simplified equation of state which is valid only in the immediate vicinity of the critical point.

In the present study, we investigate the thermodynamic consistency of LBE models developed by the forcing method by examining different numerical treatments of the LB equation. The models are applied first for the calculation of thermodynamic properties such as bulk densities, pressure, and chemical potential at various temperatures. Furthermore, the models are employed for the calculation of the interface thickness and surface tension for both planar and curved interfaces at static conditions. A comprehensive analysis of the interface properties reveals some important shortcomings of the LBE models when standard discretization schemes are used. In the framework of this analysis we propose a proper treatment that ensures thermodynamically consistent interface properties in accord with the van der Waals theory.

II. MODEL DEVELOPMENT

Following the work of He *et al.* [38] the Boltzmann equation for dense fluids can be written in the following form:

$$\frac{Df}{Dt} = \frac{\partial f}{\partial t} + \boldsymbol{\xi} \cdot \frac{\partial f}{\partial \mathbf{r}} = -\frac{1}{\lambda}(f - f^{\mathrm{eq}}) + \frac{\mathbf{F} \cdot (\boldsymbol{\xi} - \mathbf{u})}{\rho RT} f^{\mathrm{eq}}, \qquad (1)$$

where f is the single-particle distribution function, $\boldsymbol{\xi}$ is the microscopic local velocity vector of the fluid particles, $\mathbf{u}$ is the macroscopic velocity vector of the fluid, $\mathbf{r}$ is the position vector of the particles, λ is a relaxation time related to the kinematic fluid viscosity, $\mathbf{F}$ is the force experienced by the fluid particles, R is the ideal gas constant, T is the temperature, and f^{eq} is the single-particle distribution function at thermodynamic equilibrium which follows a Maxwell-Boltzmann distribution.

The forcing term $\mathbf{F}$ is expressed as

$$\mathbf{F} = \mathbf{F}_m - b\rho^2 RT\chi \nabla \ln(\rho^2 \chi) + \mathbf{G} \qquad (2)$$

and accounts for long-range ($r > \sigma$) intermolecular forces $\mathbf{F}_m$, short-range intermolecular forces ($r \leqslant \sigma$, due to the fluid

density) and body forces $\mathbf{G}$. ρ is the fluid density and χ is a density-dependent collision probability.

The forcing term associated with long-range ($r>\sigma$) intermolecular attractions is modeled in the framework of the mean-field theory in conjunction with van der Waals' gradient theory revived by Cahn-Hilliard (with the assumption that the fluid density is a slowing varying variable) employing a mean-field potential V_m [34,38,43],

$$\mathbf{F}_m = \rho \nabla V_m = \rho \nabla (2a\rho + \kappa \nabla^2 \rho) \tag{3}$$

The coefficients a, κ relate to the intermolecular potential u_{attr} as follows:

$$a = -\frac{1}{2}\int_{r>\sigma} u_{\text{attr}}(r) d\mathbf{r}, \tag{4}$$

$$\kappa = -\frac{1}{6}\int_{r>\sigma} r^2 u_{\text{attr}}(r) d\mathbf{r}. \tag{5}$$

The right-hand terms of Eq. (2) with the use of Eq. (3) can be conveniently rearranged in order to associate the forcing term $\mathbf{F}$ with the thermodynamic pressure P_0 according to [43]

$$\mathbf{F} = -[\nabla(P_0 - \rho RT)] + [\kappa\rho \nabla \nabla^2 \rho] + \mathbf{G} = -\nabla\Psi_p + \mathbf{F}_s + \mathbf{G}, \tag{6}$$

where the thermodynamic pressure satisfies the following equation of state:

$$P_0 = \rho RT(1 + b\rho\chi) - a\rho^2. \tag{7}$$

$\mathbf{G}=\rho\mathbf{g}$ is the standard gravitational body force that is normally employed to generate flow, $\mathbf{F}_s=\kappa\rho\nabla\nabla^2\rho$ is a second-order correction term arising from the implementation of the gradient theory on density and represents the force associated with surface tension and $\Psi_p=P_0-\rho RT$ is a scalar function expressing the deviation of pressure from its respective ideal gas term.

For a van der Waals fluid, the equation of state in reduced form is

$$P_0 = \frac{RT\rho}{1-b\rho} - a\rho^2, \tag{8}$$

where $b=1/3\rho_c$, $\alpha=(9/8)kT_c/\rho_c$, and $\rho_c=1$ for simplicity. It is straightforward to show that all basic quantities, such as ρ, P_0, α, b, etc., are appropriately scaled by the critical density ρ_c and the critical temperature T_c.

Then, the expression for the function Ψ_p according to [43] becomes

$$\Psi_p = \frac{RT\rho}{1-b\rho} - a\rho^2 - \rho RT, \tag{9}$$

A different rearrangement for the forcing terms in Eq. (6) has been proposed by Lee and Lin [51] in order to improve the stability of the lattice Boltzmann solution and produce a smooth pressure profile across the liquid-vapor interface,

$$\mathbf{F} = -\nabla\Psi_p' + \mathbf{F}_s' + \mathbf{G}, \tag{10}$$

where

$$\mathbf{F}_s' = \kappa\nabla(\rho\nabla^2\rho) - \frac{\kappa}{2}\nabla(\nabla\rho\cdot\nabla\rho) + \kappa\nabla(\nabla\rho\cdot\nabla\rho) - \kappa\nabla\cdot(\nabla\rho\nabla\rho) \tag{11}$$

and the scalar function Ψ_p' is calculated as

$$\Psi_p' = P_0 - \kappa\rho\nabla^2\rho + \frac{\kappa}{2}(\nabla\rho\cdot\nabla\rho) - \rho RT. \tag{12}$$

The spatial derivative of the scalar function, either $\nabla\Psi_p$ or $\nabla\Psi_p'$, is responsible for phase separation in Eq. (1).

Equation (1) can be discretized in the framework of lattice Boltzmann schemes employing a certain lattice-fluid in one, two, or three dimensions. The equilibrium distribution function is given by

$$f_i^{\text{eq}} = w_i\rho\left(1 + \frac{\boldsymbol{\xi}_i\cdot\mathbf{u}}{RT} + \frac{(\boldsymbol{\xi}_i\cdot\mathbf{u})^2}{2(RT)^2} - \frac{(\mathbf{u}\cdot\mathbf{u})}{2RT}\right), \quad i=0,N_b-1, \tag{13}$$

where w_i is a weighting factor that depends on the lattice type used in the LB model, $\boldsymbol{\xi}_i$ are the discrete velocity vectors, N_b is the number of bonds emanating from each lattice site, and i is the index of each velocity bond (for the D2Q9 LB model $N_b=9$, and so on). An in depth analysis on discretization methods of the LB equation can be found in [53–55], and references cited therein.

The most popular approach to solve Eq. (1) employs the lattice Boltzmann lagrangian-based discretization that has evolved from the lattice gas methodology. This discretization employs essentially integration along the characteristics of the lattice so that time and space discretization steps are interlinked with the velocity of the particles along the lattice, $\mathbf{c}$, $\delta\mathbf{x}=\mathbf{c}\delta t$. The resulting discretized equation in space, momentum and time is

$$f_i(\mathbf{x}+\boldsymbol{\xi}_i\delta t, t+\delta t) - f_i(\mathbf{x},t) = -\int_{\mathbf{x},t}^{\mathbf{x}+\boldsymbol{\xi}_i\delta t,t+\delta t}\frac{1}{\lambda}(f_i - f_i^{\text{eq}})dt' + \int_{\mathbf{x},t}^{\mathbf{x}+\boldsymbol{\xi}_i\delta t,t+\delta t}\frac{\mathbf{F}\cdot(\boldsymbol{\xi}_i-\mathbf{u})}{\rho RT}f_i^{\text{eq}}dt'. \tag{14}$$

Application of the trapezoidal rule in the calculation of the two integrals in Eq. (14), for second-order accuracy, results in the following equation:

$$\begin{aligned} f_i(\mathbf{x}+\boldsymbol{\xi}_i\delta t, t+\delta t) - f_i(\mathbf{x},t) &= -\frac{1}{2}\left(\frac{1}{\tau}(f_i - f_i^{\text{eq}})\right)_{\mathbf{x},t} + \frac{\delta t}{2}\left(\frac{\mathbf{F}\cdot(\boldsymbol{\xi}_i-\mathbf{u})}{RT}\Gamma_i\right)_{\mathbf{x},t} \\ &\quad -\frac{1}{2}\left(\frac{1}{\tau}(f_i - f_i^{\text{eq}})\right)_{\mathbf{x}+\boldsymbol{\xi}_i\delta t,t+\delta t} \\ &\quad +\frac{\delta t}{2}\left(\frac{\mathbf{F}\cdot(\boldsymbol{\xi}_i-\mathbf{u})}{RT}\Gamma_i\right)_{\mathbf{x}+\boldsymbol{\xi}_i\delta t,t+\delta t}, \end{aligned} \tag{15}$$

where $\Gamma_i=f_i^{\text{eq}}/\rho$ and $\tau=\lambda/\delta t$. The above equation is implicit in nature but can be made explicit by proper transformation of the distribution function f [34,38,52]. In fact the above

equation with the form of the force term given by Eq. (6) is exactly the model for nonideal fluids proposed by He *et al.* [38]. The disadvantage of the model is that the above equation is unstable and cannot be solved unless specific actions are taken. In the present study we follow two different approaches, the two-distribution function approach [43–45] and the recently proposed single-distribution function approach by Lee and Fischer with different schemes for standard and directional derivatives [52].

A. Ψ_p based, two-distribution function model (Ψ_p model)

The most common action taken to stabilize the numerical solution of Eq. (15), with the forcing expressions of Eqs. (6) or (10), is to decouple the solution for mass and momentum conservation by introducing a second distribution function $g(\mathbf{x},t)$. This function handles the conservation of momentum with the additional assumption of incompressible flow, while the first distribution function $f(\mathbf{x},t)$ solves for mass conservation.

Following [43], the particle distribution function g is defined as a function of f and the scalar function Ψ'_p from Eq. (12),

$$g = fRT - \Psi'_p(\rho)\Gamma(0). \tag{16}$$

Then, after a series of simple manipulations and further assuming incompressible flow the evolution equations of the model become

$$\bar{f}_i(\mathbf{x}+\boldsymbol{\xi}_i\delta t, t+\delta t) = \bar{f}_i(\mathbf{x},t) - \frac{\bar{f}_i(\mathbf{x},t) - f_i^{\mathrm{eq}}(\mathbf{x},t)}{\tau'} + \frac{2\tau'-1}{\tau'}\frac{(\boldsymbol{\xi}_i-\mathbf{u})\cdot\mathbf{F}}{RT}\Gamma_i(\mathbf{u})\delta t \tag{17a}$$

and

$$\bar{g}_i(\mathbf{x}+\boldsymbol{\xi}_i\delta t, t+\delta t) = \bar{g}_i(\mathbf{x},t) - \frac{\bar{g}_i(\mathbf{x},t) - g_i^{\mathrm{eq}}(\mathbf{x},t)}{\tau'} - \frac{2\tau'-1}{\tau'}(\boldsymbol{\xi}_i-\mathbf{u})\cdot\{\Gamma_i(\mathbf{u})(\mathbf{F}'_s+\mathbf{G}) - [\Gamma_i(\mathbf{u})-\Gamma_i(\mathbf{0})]\nabla\Psi'_p\}\delta t, \tag{17b}$$

where $\tau' = \tau + 1/2$ and the redefined distribution functions $\bar{f}$, $\bar{g}$ are given by

$$\bar{f}_i = f_i - \frac{(\boldsymbol{\xi}_i-\mathbf{u})\cdot\mathbf{F}}{2RT}\Gamma_i(\mathbf{u})\delta t, \tag{18a}$$

$$\bar{g}_i = g_i - \frac{1}{2}(\boldsymbol{\xi}_i-\mathbf{u})\cdot\{\Gamma_i(\mathbf{u})(\mathbf{F}'_s+\mathbf{G}) - [\Gamma_i(\mathbf{u})-\Gamma_i(0)]\nabla\Psi'_p\}\delta t. \tag{18b}$$

Note that the forcing term $\mathbf{F}$ for the evolution equation for $\bar{f}$ can be calculated by either Eq. (6) or Eq. (10). Our results have shown that the selection of $\mathbf{F}$ for the evolution equation for $\bar{f}$ has a negligible effect. Therefore, we selected to use Eq. (6) for compatibility with the work of Lee and Lin [51], while the expression of Eq. (10) in used for the computations of the evolution equation for $\bar{g}$.

The density and velocity vector are calculated by the following expressions:

$$\rho = \sum_i \bar{f}_i, \tag{19}$$

$$RT\rho\mathbf{u} = \sum_i \bar{g}_i\boldsymbol{\xi}_i + \frac{RT\delta t}{2}(\mathbf{F}'_s+\mathbf{G}). \tag{20}$$

Finally the hydrodynamic pressure, P, can be calculated separately from the first moment of the distribution function $\bar{g}$,

$$P = \sum_i \bar{g}_i - \frac{1}{2}\mathbf{u}\cdot\nabla\Psi'_p\delta t. \tag{21}$$

All derivatives (both directional and nondirectional) are calculated using a central isotropic discretization scheme according to [51,52] in order to improve stability and preserve the second-order accuracy of the whole numerical solution,

$$\nabla\rho|_{(\mathbf{x})} = \sum_{i\neq 0}\frac{w_i\boldsymbol{\xi}_i[\rho(\mathbf{x}+\boldsymbol{\xi}_i\delta t)-\rho(\mathbf{x}-\boldsymbol{\xi}_i\delta t)]}{2RT\delta t}, \tag{22a}$$

$$\nabla^2\rho|_{(\mathbf{x})} = \sum_{i\neq 0}\frac{w_i[\rho(\mathbf{x}+\boldsymbol{\xi}_i\delta t)-2\rho(\mathbf{x})+\rho(\mathbf{x}-\boldsymbol{\xi}_i\delta t)]}{RT\delta t^2}. \tag{22b}$$

B. Gibbs-Duhem based, two-distribution function model (Gibbs-Duhem model)

It has been argued before [50] that the Ψ_p model proposed by He *et al.* [38] (see Sec. II A) does not accurately predict the true equilibrium densities as can be determined by the Maxwell equal area rule, at a certain temperature. A major reason for the above problem is the fact that the forcing model does not account for the effect of chemical potential at equilibrium. The model establishes mechanical equilibrium ($P_l = P_g$) but not chemical equilibrium where the chemical potentials of the two phases, μ_l and μ_g, are equal. This is because it has not been possible to devise a proper discrete gradient operator ∇ such that the Gibbs-Duhem equation $\nabla P_0 = \rho\nabla\mu_0$, which determines phase equilibrium, holds exactly [50]. The subscript 0 denotes properties at the bulk fluid phases away from fluid-fluid interfaces.

For this reason, Lee and co-workers [51,52] proposed the following modification in Eq. (6) by introducing the Gibbs-Duhem equation, replacing ∇P_0 by $\rho\nabla\mu_0$. Then assuming that there is no gravitational or other body forces present, Eq. (6) becomes

$$\mathbf{F} = \nabla\rho RT - \rho\nabla(\mu_0 - \kappa\nabla^2\rho) = \nabla\rho RT - \rho\nabla\mu, \tag{23}$$

where $\mu = \mu_0 - \kappa\nabla^2\rho$ in accord with van der Waals theory and its successors [2–4].

The bulk chemical potential μ_0 for a fluid that obeys the van der Waals equation of state is found by solving the equation for the bulk energy density E_0 [1],

$$P_0 = \rho\mu_0 - E_0, \quad \text{where } \mu_0 = \frac{\partial E_0}{\partial \rho}. \tag{24}$$

We take

$$\mu_0 = \frac{RT\ln\rho}{1-b\rho} + \frac{RT}{1-b\rho} - 2a\rho \tag{25}$$

or in the general case, where an interface may be present

$$\mu = \frac{RT\ln\rho}{1-b\rho} + \frac{RT}{1-b\rho} - 2a\rho - \kappa\nabla^2\rho. \tag{26}$$

The above model can be successfully employed using the two-distribution function approach in a similar way with the Ψ_p model presented in Sec. II A. The evolution equations for this model are Eqs. (17a) and (17b), but the forcing term for Eq. (17a) is given by Eq. (23), while the forcing term for Eq. (17b) is given by Eq. (10), as in Sec. II A. The density, pressure, and velocity are calculated as in Sec. II A.

C. Ψ_μ based, two-distribution function model (Ψ_μ model)

In the present study we propose to replace ∇P_0 by $\rho\nabla\mu_0$, in a similar fashion with the Gibbs-Duhem model (see Sec. II B), but then proceed differently in the formulation of $\mathbf{F}$. We define the function $\Psi_\mu(\mathbf{x},t)$ as the deviation of the chemical potential from its respective ideal gas term, μ^{ideal} [56],

$$\Psi_\mu = \mu - \mu^{\text{ideal}}. \tag{27}$$

Thus, given the chemical potential of the ideal gas, we have

$$\nabla\Psi_\mu = \nabla(\mu - RT\ln\rho). \tag{28}$$

The forcing term from Eq. (23) (assuming again $\mathbf{G}=\mathbf{0}$) can be expressed in terms of Ψ_μ as follows:

$$\mathbf{F} = -\rho\nabla\Psi_\mu = -\rho\nabla\mu_0 + \rho RT\nabla\ln\rho + \kappa\rho\nabla\nabla^2\rho. \tag{29}$$

In essence, the proposed model employs the Gibbs-Duhem thermodynamic equation at the Ψ level (and not in μ and ρ level) resulting in a different discretization of the phase equilibrium equation compared to the standard Gibbs-Duhem model developed in the section above. The two-distribution function approach is also employed in the proposed model in exactly the same way as with the other two models. The evolution equations are Eqs. (17a) and (17b) but the forcing term for Eq. (17a) is given by Eq. (29). The forcing term $\mathbf{F}$ for the evolution equation for $\bar{g}$ [Eq. (17b)] is given by Eq. (10), as in all previous models (see Sec. II A and II B).

D. Lee-Fischer, single-distribution function model (Lee-Fischer model)

Lee and Fischer [52] adopted the concept of employing Gibbs-Duhem equation in the forcing term but they handled successfully the stability challenges of single-distribution function models at large density ratios by proposing proper compact isotropic discretizations for the directional $(\boldsymbol{\xi}_i\cdot\nabla)$ and nondirectional derivatives (∇) in the forcing terms.

The single-distribution function model by Lee and Fischer employs the following evolution equation:

$$\bar{f}_i(\mathbf{x}+\boldsymbol{\xi}_i\delta t, t+\delta t) - \bar{f}_i(\mathbf{x},t) = -\left(\frac{1}{\tau}(\bar{f}_i - \bar{f}_i^{\text{eq}})\right)_{\mathbf{x},t} + \frac{(\boldsymbol{\xi}_i - \mathbf{u})\cdot(\nabla^M\rho RT - \rho\nabla^M\mu)}{\rho RT} \times f_i^{\text{eq}}(\mathbf{x},t)\,\delta t, \tag{30}$$

where

$$\bar{f}_i^{\text{eq}} = f_i^{\text{eq}} - \frac{\delta t}{2}\frac{(\boldsymbol{\xi}_i - \mathbf{u})\cdot(\nabla^C\rho RT - \rho\nabla^C\mu)}{\rho RT} f_i^{\text{eq}} \tag{31}$$

and

$$\nabla^M\rho|_{(\mathbf{x})} = \frac{1}{2}[\,\nabla^C\rho|_{(\mathbf{x})} + \nabla^B\rho|_{(\mathbf{x})}], \tag{32a}$$

$$\delta t\boldsymbol{\xi}_i\cdot\nabla^M\rho|_{(\mathbf{x})} = \frac{1}{2}[\,\delta t\boldsymbol{\xi}_i\nabla^C\rho|_{(\mathbf{x})} + \delta t\boldsymbol{\xi}_i\nabla^B\rho|_{(\mathbf{x})}]. \tag{32b}$$

This mixed scheme considers an equal contribution of central and biased finite differences. For the case of directional derivatives the following second-order schemes are used for central and biased differences respectively:

$$\delta t\boldsymbol{\xi}_i\cdot\nabla^C\rho|_{(\mathbf{x})} = \frac{\rho(\mathbf{x}+\boldsymbol{\xi}_i\delta t) - \rho(\mathbf{x}-\boldsymbol{\xi}_i\delta t)}{2}, \tag{33a}$$

$$\delta t\boldsymbol{\xi}_i\cdot\nabla^B\rho|_{(\mathbf{x})} = \frac{-\rho(\mathbf{x}+2\boldsymbol{\xi}_i\delta t) + 4\rho(\mathbf{x}+\boldsymbol{\xi}_i\delta t) - 3\rho(\mathbf{x})}{2}. \tag{33b}$$

Derivatives other than directional are computed by taking moments of the one-dimensional (1D) finite difference schemes with appropriate weights to yield isotropic discretizations,

$$\nabla^C\rho|_{(\mathbf{x})} = \sum_{i\neq 0}\frac{w_i\boldsymbol{\xi}_i[\rho(\mathbf{x}+\boldsymbol{\xi}_i\delta t) - \rho(\mathbf{x}-\boldsymbol{\xi}_i\delta t)]}{2RT\delta t}, \tag{34a}$$

$$\nabla^B\rho|_{(\mathbf{x})} = \sum_{i\neq 0}\frac{w_i\boldsymbol{\xi}_i[-\rho(\mathbf{x}+2\boldsymbol{\xi}_i\delta t) + 4\rho(\mathbf{x}+\boldsymbol{\xi}_i\delta t) - 3\rho(\mathbf{x})]}{2RT\delta t}, \tag{34b}$$

$$\nabla^2\rho|_{(\mathbf{x})} = \sum_{i\neq 0}\frac{w_i[\rho(\mathbf{x}+\boldsymbol{\xi}_i\delta t) - 2\rho(\mathbf{x}) + \rho(\mathbf{x}-\boldsymbol{\xi}_i\delta t)]}{RT\delta t^2}. \tag{34c}$$

Accordingly, density and velocity vector are determined taking the moments of the distribution function resulting in the following expressions:

$$\rho = \sum_i \bar{f}_i, \tag{35}$$

$$\mathbf{u} = \sum_i \bar{f}_i \boldsymbol{\xi}_i / \rho + \frac{\delta t}{2}(\boldsymbol{\nabla}^C \rho RT - \rho \boldsymbol{\nabla}^C \mu). \tag{36}$$

In the present study we will consider two different schemes: The standard equal-weight mixed finite difference scheme (Lee-Fischer M model) also employed in [52] and a fully central finite difference (Lee-Fischer C model) scheme to examine the effect of derivative discretization.

III. RESULTS AND DISCUSSION

A. Planar interface

Our first aim is to explore whether the models examined can correctly reproduce the bulk thermodynamic properties of a vdW fluid at different temperatures. Hence, we first performed 1D simulations at a planar interface. In all cases we used 200 lattice units in the axial direction where 60 units at each end contained gas phase molecules and the rest 80, located at the center, contained liquid phase molecules. We always started from the thermodynamic gas and liquid densities computed from the Maxwell construction curve at a specific T/T_c, although we have also performed studies starting from different initial densities to ensure uniqueness of the solution. The D1Q3 scheme was used while additional simulations were performed with the D2Q9 model.

In order to study the effect of the second-order density gradient in the mean-field potential and hence in the forcing term associated with long-range intermolecular attractions, parameter κ must get nonzero values. However, based on the definition of κ [Eq. (5)] it is evident that this parameter cannot get arbitrary values and must be related to the vdW equation of state through the attraction parameter a, and a proper intermolecular interaction model.

Looking at the definitions of the parameters a and κ [Eqs. (4) and (5)] it is evident that both parameters depend on the type of attraction part of the intermolecular interaction model. For a Lennard-Jones fluid it follows

$$U(r) = 4\varepsilon\left[\left(\frac{\sigma}{r}\right)^{12} - \left(\frac{\sigma}{r}\right)^{6}\right], \tag{37}$$

where $U(r)$ is the potential energy of interaction, r is the intermolecular distance, σ is the molecular (collision) diameter, and ε is an energy parameter corresponding to the depth of the potential well.

From this equation it follows that $u_{\mathrm{attr}}(r) = -4\varepsilon(\frac{\sigma}{r})^6$, which upon substitution in Eqs. (4) and (5) gives the following expressions for a and κ:

$$a = \frac{8\pi\sigma^3\varepsilon}{3}, \tag{38a}$$

$$\kappa = \frac{8\pi\sigma^5\varepsilon}{3}. \tag{38b}$$

Thus it is straightforward to show that for the specific potential we have

$$\kappa = a\sigma^2. \tag{39}$$

Note that in the present study we have considered a certain type of Lennard-Jones potential, although there are several variants of it. In all cases the only thing that will change is the numerical factor that relates parameters κ and a, which will still be of the order $O(1)$.

In order to examine the effect of the lattice spacing or pixel size δx on the interfacial properties, we write the field potential in Eq. (3) as follows:

$$V_m = 2a\rho + \tilde{\kappa}\tilde{\nabla}^2\rho, \tag{40}$$

where

$$\tilde{\kappa} = a\left(\frac{\sigma}{\delta x}\right)^2 \tag{41}$$

and

$$\boldsymbol{\nabla} = \frac{1}{\delta x}\tilde{\boldsymbol{\nabla}}. \tag{42}$$

There are several other approaches that are fully equivalent depending on the solution procedure followed in each case [5,57]. With this approach the parameter $\tilde{\kappa}$ gives a measure of the process scale. Thus if the pixel size δx is of the order of many molecular diameters (large scale) then $\tilde{\kappa} \to 0$ and consequently $\tilde{\nabla}^2\rho \to \infty$. In this scale the interface thickness should tend to zero as it is when we "look" at a two-phase system on the macroscale and the addition of the second-order density gradient is not important in Eqs. (6), (23), and (29). On the other hand, as the pixel size δx approaches the value of the molecular diameter σ, then $\tilde{\kappa} \to a$ and in this case the interface thickness is expected to have finite values since it is known both from theoretical and experimental studies that the interface thickness is of the order of a few molecular diameters and further increases with appropriate scaling relations as the system approaches its critical temperature [58–60].

In order to study the effect of κ in a systematic way we varied δx from 4σ το σ. This means that $\tilde{\kappa}$ varied from $a/16$ up to a.

1. Two-distribution function models

Our first set of simulations involved the determination of the phase diagram for a van der Waals fluid using the different models discussed above. In all cases we used the two-distribution function concept of He *et al.* [43] with the additional assumption of incompressible flow and the modifications in the calculation for $\mathbf{F_s}$ introduced by Lee and Lin [51] [see also Eq. (11)]. The results for $\delta x = 4\sigma$ and $\delta x = \sigma$ are presented in Fig. 1. Looking at the results of Fig. 1(a), it is evident that for pixel sizes $\delta x = 4\sigma$ ($\tilde{\kappa} = a/16$) the two-distribution LBM models cannot predict very accurately the equilibrium gas and liquid densities for $T/T_c < 0.98$. The Ψ_p model gives the worst predictions among the different models while the Ψ_μ model gives the best ones extending the region of validity to $T/T_c > 0.93$. On the other hand, as we decrease the pixel size to $\delta x = \sigma$ ($\tilde{\kappa} = a$) the results in Fig. 1(b) are significantly improved and predictions of all three

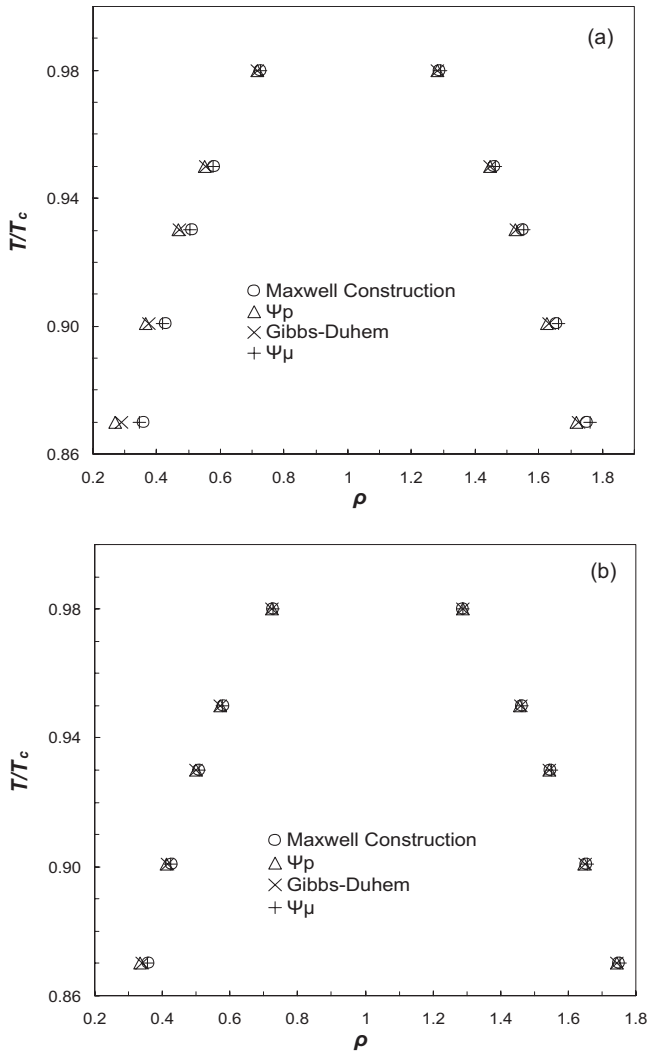

FIG. 1. Phase diagram calculations for a van der Waals fluid using two-distribution function LBE models. (a) $\delta x=4\sigma$ ($\tilde{\kappa}=a/16$) and (b) $\delta x=\sigma$ ($\tilde{\kappa}=a$).

models are in much closer agreement with the exact thermodynamic values of the phase diagram, compared to the respective results obtained at $\delta x=4\sigma$. Further to the above results, all models produce zero spurious velocities (down to machine accuracy) regardless of the value of δx (and hence κ). This result implies that spurious velocity is not the only factor that affects the thermodynamic consistency of the LBM models.

The results on the thermodynamic pressure P_0 [calculated by Eq. (8)] on the bulk gas and liquid sides for two different temperatures ($T/T_c=0.9009$ and $T/T_c=0.98$) for the Ψ_μ model are presented in Fig. 2. This figure shows that there is a threshold value of $\tilde{\kappa}$ at each temperature above which, we can establish true thermodynamic equilibrium in the system. Similar results are obtained when plotting the bulk chemical potential μ_0 [calculated by Eq. (25)] vs $\tilde{\kappa}$. Similar trends have been shown in previous studies [48–50]. However, in these studies $\tilde{\kappa}$ was varied arbitrarily, while in the present study we have been able to relate the magnitude of $\tilde{\kappa}$ with the equation of state of the fluid and the size of the lattice spacing.

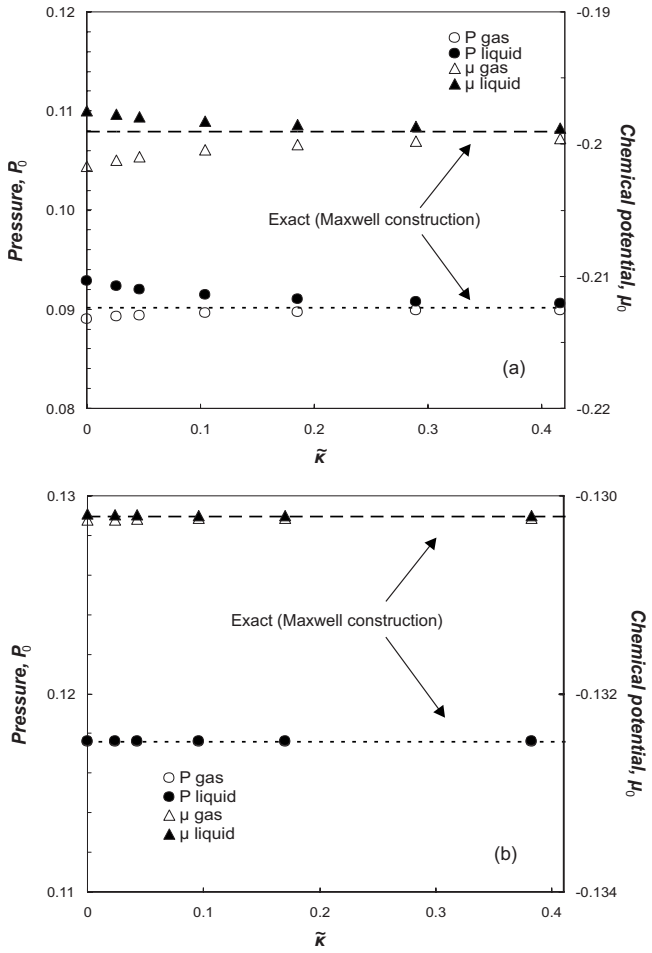

FIG. 2. Effect of density gradient parameter $\tilde{\kappa}$ on the thermodynamic pressure, P_0, and chemical potential, μ_0, at the bulk liquid (black symbols) and gas phase (open symbols) at two different temperatures: (a) $T/T_c=0.9009$ and (b) $T/T_c=0.98$ (Ψ_μ model).

These results show that we can reach thermodynamic equilibrium by decreasing the pixel size accordingly (if necessary going down to molecular scale, in accord with the findings of Horbach and Succi [61]). It is also interesting to see if this trend is followed by the other models. Thus in Fig. 3 we present the respective plots for pressure and chemical potential vs $\tilde{\kappa}$, for the Ψ_p model, while in Fig. 4 the same plots are given for the case of the Gibbs-Duhem two-distribution model. In both cases we observe similarities as well as some noticeable differences compared to the proposed model. First of all, both models cannot attain exact thermodynamic equilibrium dictated by Maxwell's construction, unless $\tilde{\kappa}$ reaches a certain threshold value (and hence resolution becomes fine enough) at a specific temperature, in accord with the results obtained for the Ψ_μ model. On the other hand, both Ψ_p and Gibbs-Duhem models are always at mechanical equilibrium (but not at chemical equilibrium), while the Ψ_μ model reaches both mechanical and chemical equilibrium at more or less the same threshold value of $\tilde{\kappa}$. This trend is seen at all temperatures examined in the present study, with the differences among the models becoming smaller as T/T_c approaches unity.

From the results of Figs. 1–4, it is evident that the bulk property predictions of all models can become thermody-

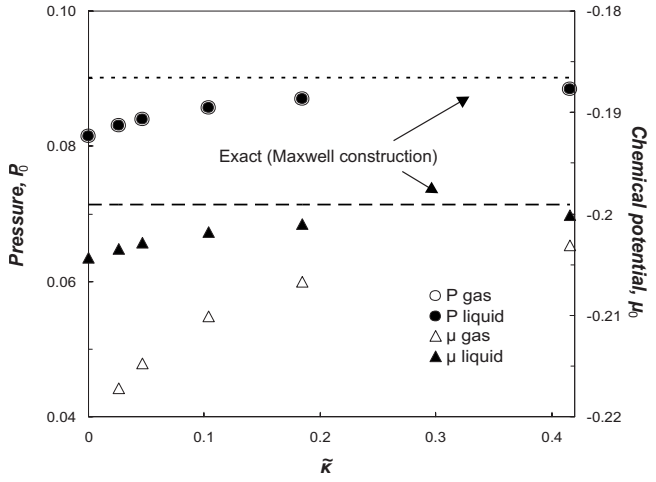

FIG. 3. Effect of density gradient parameter $\tilde{\kappa}$ on the thermodynamic pressure, P_0, and chemical potential, μ_0, at the bulk liquid (black symbols) and gas phase (open symbols) at $T/T_c=0.9009$ (Ψ_p model).

namically consistent by proper fine-tuning of the resolution (i.e., by appropriately reducing the pixel size δx). In fact, the present results indicate that if we are not in the immediate vicinity of the critical temperature, T_c, then we must work with a resolution of the order of the molecular diameter in order to obtain thermodynamically consistent results when using the two-distribution function models.

2. Lee-Fischer, single-distribution function model

We next repeat the previous calculations using the single-distribution function model developed by Lee and Fischer [52]. The calculations have been performed using a fully central finite difference scheme (Lee-Fischer model *C*) and a mixed finite difference scheme for both directional and nondirectional derivatives (Lee-Fischer model *M*). Directional derivatives are calculated by Eqs. (32b), (33a), and (33b),

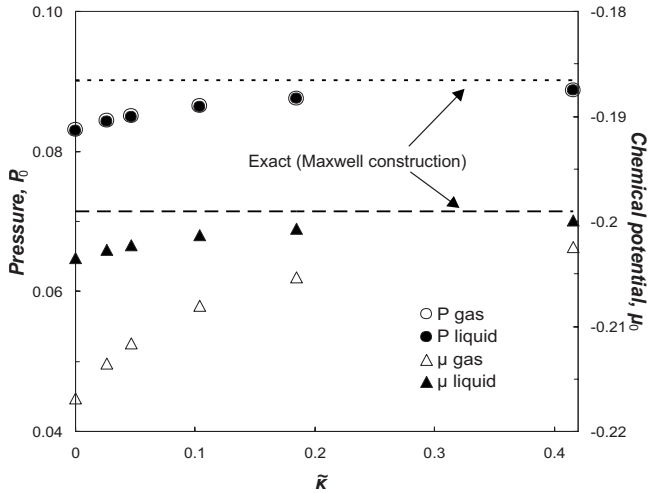

FIG. 4. Effect of density gradient parameter $\tilde{\kappa}$ on the thermodynamic pressure, P_0, and chemical potential, μ_0, at the bulk liquid (black symbols) and gas phase (open symbols) at $T/T_c=0.9009$ (Gibbs-Duhem model).

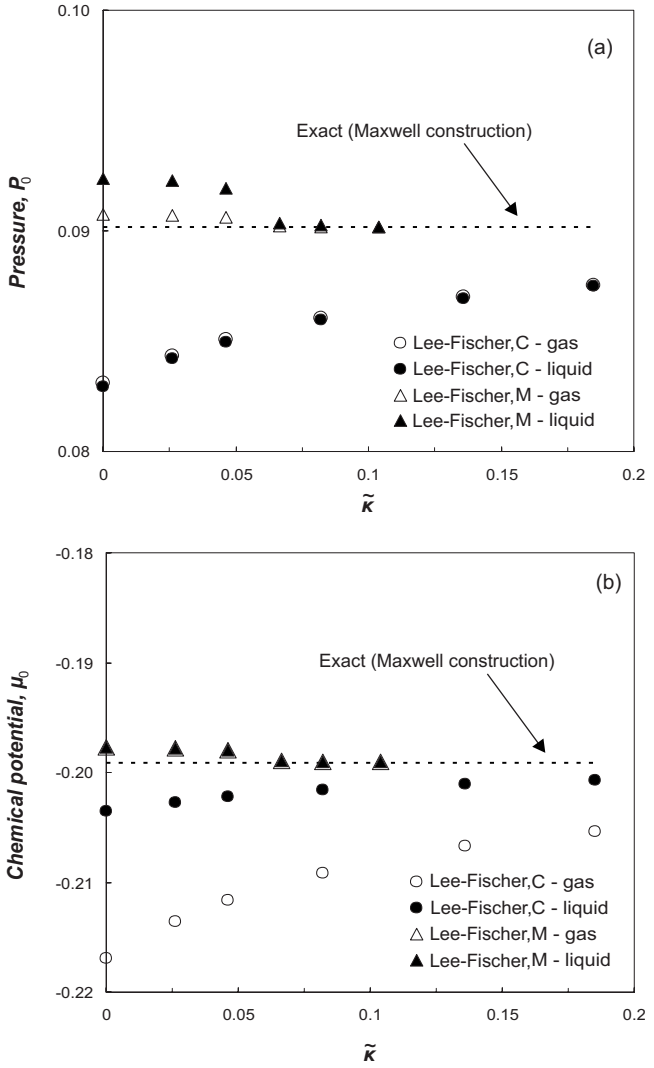

FIG. 5. Effect of density gradient parameter $\tilde{\kappa}$ (a) on the thermodynamic pressure, P_0, and (b) chemical potential, μ_0, at the bulk liquid (black symbols) and gas phase (open symbols) at $T/T_c=0.9009$ using the single-distribution function model of Lee and Fischer [52].

while nondirectional derivatives are calculated by Eqs. (32a), (34a), and (34b). Additional calculations have shown that the type of the finite difference scheme, whether it is mixed or fully central, has a negligible effect in the nondirectional derivatives, as long as isotropic schemes are employed, in accord with previous studies [51,52].

In Fig. 5 we present the respective plots for pressure and chemical potential vs $\tilde{\kappa}$ at two different temperatures for the Lee-Fischer model *C* and the Lee-Fischer model *M*. Looking at these results several interesting conclusions can be drawn: First the fully central finite difference scheme produces almost identical results with the respective two-distribution function (Gibbs-Duhem) model. The mixed finite difference scheme model, on the other hand, shows an excellent agreement with the exact thermodynamic results at much lower resolutions ($\delta x \sim 3\sigma$). It must be noted that the Lee-Fischer model *M* shows some instabilities at very high resolutions ($\delta x < 2\sigma$) while the fully central finite difference scheme re-

mains stable. In all cases the maximum spurious velocity is very low of the order of 10^{-14}–10^{-15} in accord with the original study of Lee and Fischer [52].

It must be noted that we have performed additional simulations using Eq. (29) instead of Eq. (23) in the Lee-Fischer one-distribution model. We observe almost identical results with the ones obtained with the respective two-distribution function model (Ψ_μ model) when using the fully central finite difference scheme for the directional derivatives (C model). However, when using the mixed finite difference scheme (M model) the model becomes unstable after a sufficiently large number of time steps and cannot be further evaluated in this case. Nevertheless, it must be noted that the purpose of employing Eq. (29) as an alternative form of the Gibbs-Duhem model was to introduce a more appropriate form of the Ψ function in the two-distribution function models. It is evident that for the case of one-distribution function models the approach of Lee and Fischer [52] is by far the most appropriate one, when mixed schemes are used for the discretization of the directional derivatives.

B. Interface thickness

In our simulations so far we have not discussed in detail the thickness of the interface. According to the van der Waals theory, the interface thickness, ℓ, can be determined by numerically solving the following integral for the case of a planar interface [5,57]:

$$\ell^* = x^* - x_0^* = -\frac{1}{\sqrt{2}} \int_{\rho^*(x_0^*)}^{\rho^*(x^*)} \frac{d\rho^*}{[\Phi^*(\rho^*) - \Phi^*(\rho_l^*)]^{1/2}}, \quad (43)$$

where $\ell^* = \ell(\frac{a}{\kappa})^{1/2} = \ell/\sigma$, $x^* = (\frac{a}{\kappa})^{1/2} = x/\sigma$, $\rho^* = \rho b$, $T^* = bRT/a$,

$$\Phi^* = \rho^* \zeta - \rho^* T^* [\ln(1/\rho^* - 1) + 1] - \rho^{*2}, \quad (44a)$$

$$\zeta = T^* \ln(1/\rho^* - 1) - \frac{\rho^* T^*}{1 - \rho^*} + 2\rho^*. \quad (44b)$$

The above integral can be solved numerically in a straightforward manner [5]. Note that the solution of the above equations gives the exact density profile for a planar interface for any value of T/T_c. In the case that T is in the vicinity of the critical point, we can obtain the analytic expression that employs the hyperbolic tangent function to relate density with distance and interface thickness using scaling arguments [60]. It must be stated however that the latter expression is strictly valid only for $T/T_c > 0.99$, leaving a very limited temperature range and often serves as a fitting expression [60].

An additional result from the thermodynamic theory of interfaces is that at temperatures close to the critical one, parameter $\tilde{\kappa}$ scales with the square of the interface thickness, ℓ, namely $\tilde{\kappa} \propto \ell^2$ and $\ell = 0$ when $\tilde{\kappa} = 0$ [1,2]. This is a point we have already touched upon when we nondimensionalized κ, since at large scales the lattice spacing is of the order of many molecular diameters ($\tilde{\kappa} \to 0$) and the interface thickness should tend to zero as it is when we "look" at a two-phase system at these scales. As a first step we consider a planar interface and proceed by calculating the interface thickness, ℓ, as a function of parameter $\tilde{\kappa}$ using the different models. The midpoint method was used to calculate ℓ in accord with previous studies [1].

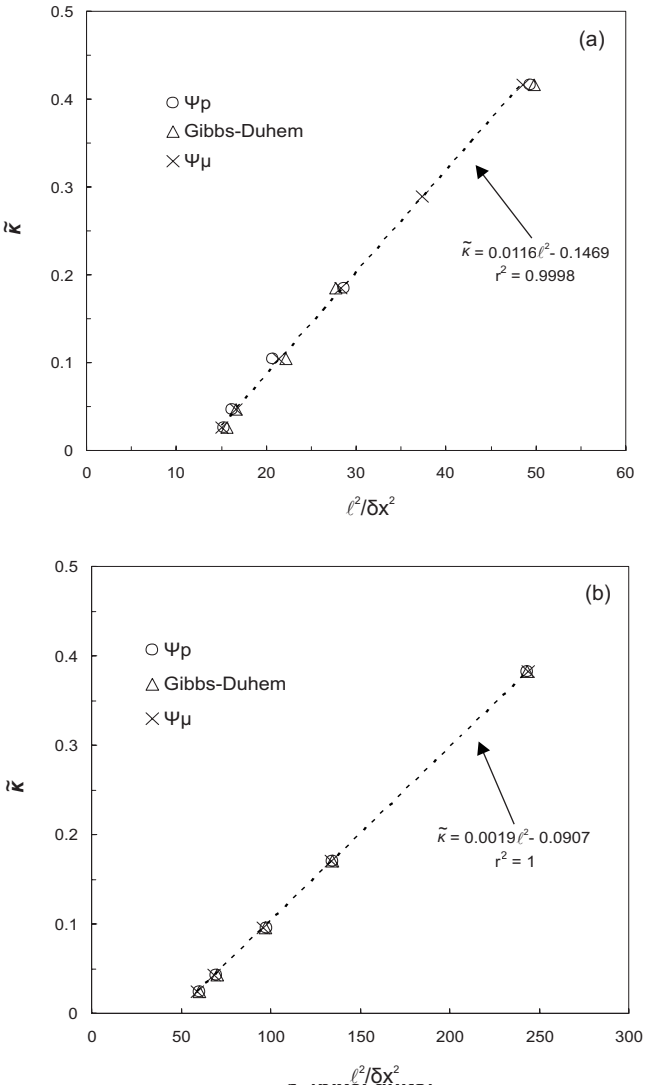

FIG. 6. Dependence of the interface thickness ℓ (in lattice units, δx) on density gradient parameter $\tilde{\kappa}$, using the two-distribution function models, at two different temperatures: (a) $T/T_c = 0.9009$ and (b) $T/T_c = 0.98$.

1. Two-distribution function models

The results for the two-distribution function models are illustrated in Fig. 6 indicating a perfect linear fit between $\tilde{\kappa}$ and ℓ^2 in accord with the respective thermodynamic theory. The only difference is that at $\ell = 0$ we get a nonzero value for $\tilde{\kappa}$. This implies that the two-distribution function LBE models show an artificial surface tension (due to the nonzero value of $\tilde{\kappa}$ at $\ell = 0$). It is noteworthy that all models produce almost identical results indicating that the interface thickness does not seem to be affected by whether the Gibbs-Duhem expression is employed or how it is employed in the LBE model. This result prompted us to assume that we can "absorb" the nonzero value of $\tilde{\kappa}$ at zero thickness into the nomi-

TABLE I. Apparent and corrected values for parameter $\tilde{\kappa}$ and pixel size δx.

T/T_c=0.9009		Ψ_μ model	
$\tilde{\kappa}$	$\delta x/\sigma$	$\tilde{\kappa}_{\mathrm{cor}}$	$\delta x_{\mathrm{cor}}/\sigma$
0	∞	0.1506	1.66
0.0260	4	0.1766	1.54
0.0463	3	0.1969	1.45
0.1041	2	0.2547	1.28
0.1850	1.5	0.3356	1.11
0.4163	1	0.5669	0.86

nal value of $\tilde{\kappa}$ that we use as an input parameter in our models. This will result in a recalculation of the value of the pixel size simply working in a reverse manner starting from Eq. (41). The respective calculations for the Ψ_μ model are summarized in Tables I and II for T/T_c 0.9009 and 0.98, respectively. It is seen that the corrected pixel sizes are now shifted to only a few molecular sizes even when $\tilde{\kappa}$=0, due to the artificial surface tension effect. Similar results are found when any of the other two-distribution function models are employed. This is an important result that reveals the size limitations of the two-distribution function LBE models. It is evident that these models cannot be employed to simulate two-phase flow phenomena at the macroscale unless of course one uses extremely large domains.

The calculations shown in Tables I and II can be further employed to "correct" the calculation of the interface thickness in units of molecular diameter, σ. Thus we proceeded with the evaluation of the interface thickness in σ units (and not in pixels) for different values of the nominal parameter $\tilde{\kappa}$. The results are shown in Fig. 7, including the exact solution of van der Waals theory for interfaces, resulting upon integration of Eq. (43).

From these results we can see that the predictions for the interface thickness deviate from the exact solution from van der Waals theory for interfaces and the deviation is less as we increase the value of $\tilde{\kappa}$ or, equivalently, as we decrease the lattice spacing (i.e., increasing the resolution). On the other hand, when correcting $\tilde{\kappa}$ by adding its respective value at the ordinate and redefining the value of the lattice spacing accordingly from Eq. (41), we end up with predictions for the interface thickness that are in excellent agreement with the van der Waals theory for interfaces, even at the low resolutions (low $\tilde{\kappa}$ values). Moreover, the predictions become better as we get closer to the critical temperature, where the interfaces are smoother and so the effect of artificial surface tension is not as important as in lower temperatures.

TABLE II. Apparent and corrected values for parameter $\tilde{\kappa}$ and pixel size δx.

T/T_c=0.98		Ψ_μ model	
$\tilde{\kappa}$	$\delta x/\sigma$	$\tilde{\kappa}_{\mathrm{cor}}$	$\delta x_{\mathrm{cor}}/\sigma$
0	∞	0.0970	2.05
0.0239	4	0.1146	1.83
0.0425	3	0.1332	1.70
0.0957	2	0.1864	1.43
0.1701	1.5	0.2608	1.21
0.3827	1	0.4734	0.90

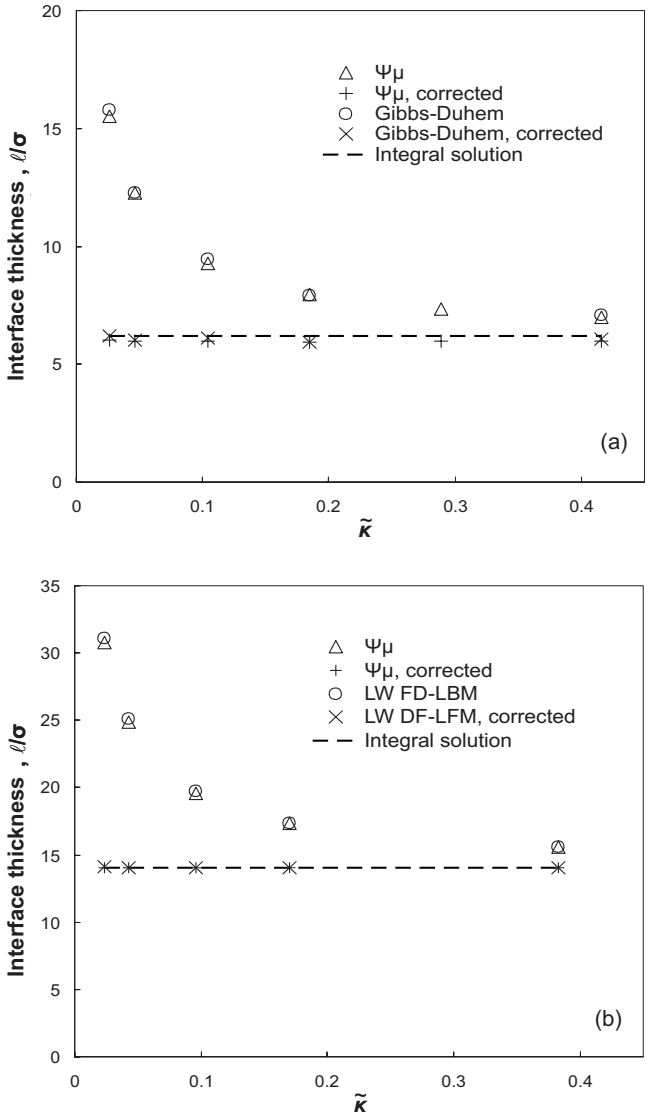

FIG. 7. Dependence of the interface thickness, in σ units, on density gradient parameter $\tilde{\kappa}$, using the two-distribution function models with and without correction, at two different temperatures: (a) T/T_c=0.9009 and (b) T/T_c=0.98.

In all cases examined, the lattice spacing employed is of the order of a few molecular diameters. Thus, the proposed methodology, although it "corrects" the validity of the two-distribution function LBE models, it cannot completely "cure" them since it is obvious that if one works with pixel sizes of the order of 100 σ (so that $\tilde{\kappa}\rightarrow 0$) the interface thickness will not be as thin as it should be, simply because there is a lower limit in the value of parameter $\tilde{\kappa}$, dictated by its value at the ordinate. This limits the selection of the pixel size to values that can predict the interface thickness correctly, while also predicting correctly the thermodynamic gas and liquid density values. The apparent problem can be

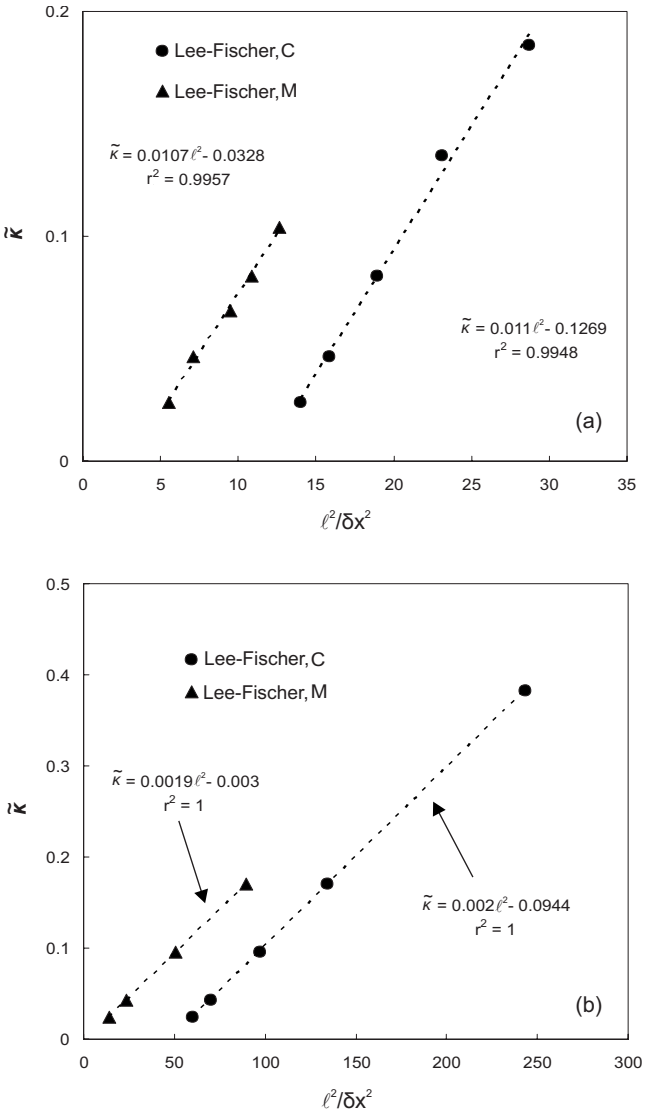

FIG. 8. Dependence of the interface thickness ℓ (in lattice units, δx) on density gradient parameter $\tilde{\kappa}$, using the single-distribution function model of Lee and Fischer, at two different temperatures: (a) T/T_c=0.9009, and (b) T/T_c=0.98.

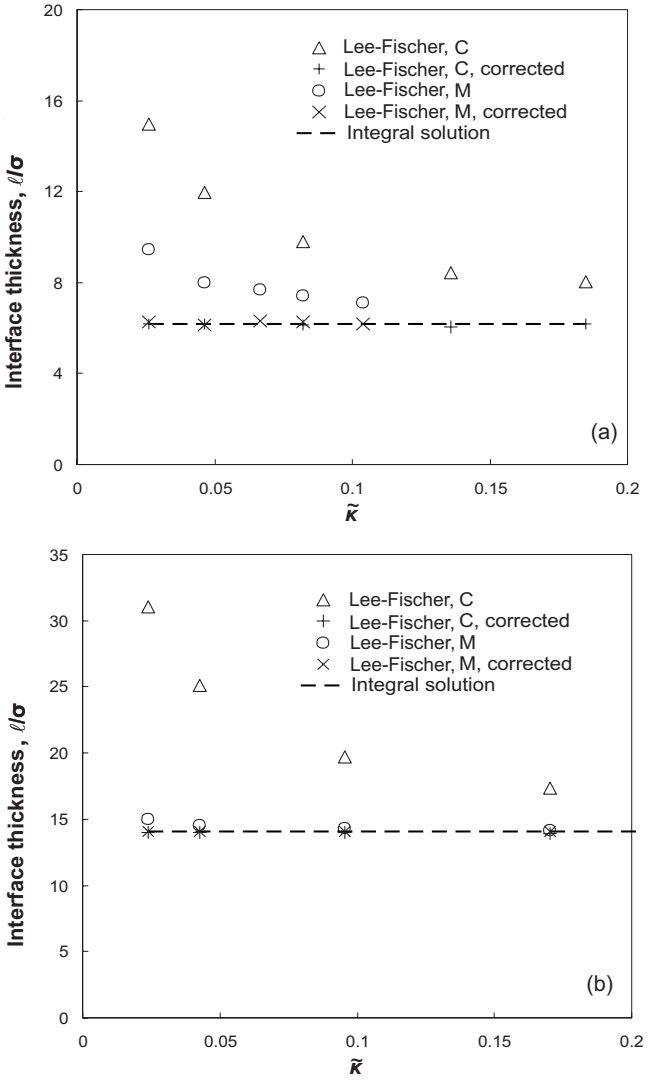

FIG. 9. Dependence of the interface thickness, in σ units, on density gradient parameter $\tilde{\kappa}$, using the single-distribution function model of Lee and Fischer, with and without correction, at two different temperatures: (a) T/T_c=0.9009 and (b) T/T_c=0.98.

"solved" by increasing the system size accordingly, something that can be tolerated up to a point given the ease of parallelization of LBM methods.

2. Lee-Fischer, single-distribution function model

The results for the Lee-Fischer single-distribution function LBE model are illustrated in Fig. 8. In Fig. 8 we have included the predictions for the Lee-Fischer model *C*, and the Lee-Fischer model *M*. It is evident that both models predict a perfect linear fit between $\tilde{\kappa}$ and ℓ^2 with almost identical slopes that are also in close agreement with the ones produced by the two-distribution function models (see also Fig. 6). Moreover, the central model shows a nonzero ordinate due to the artificial surface tension effect, that is quantitatively the same with the respective result for the two-distribution function models. The mixed model on the other hand shows practically no artificial surface tension with a negligible correction for $\tilde{\kappa}$. The only limitation of the mixed model is a loss of stability at very sharp interfaces (below 3–4 pixels) and/or very high resolutions ($\delta x < 2\sigma$). Following the same methodology employed in the preceding section we compare in Fig. 9 the predictions of the Lee-Fischer single-distribution function LBE model on the interface thickness with the results from the exact solution from van der Waals theory for interfaces. Once again a corrected value for $\tilde{\kappa}$ (and thus a corrected value for the lattice spacing size δx) must be used for the case of the central model in order to match the exact interface thickness, while this correction is negligible for the mixed model even at the lower temperature of T/T_c=0.9009. It is evident that the mixed finite difference scheme is the one that controls the accuracy of the interface thickness by minimizing the effect of artificial surface tension. Unfortunately the mixed model shows some stability limitations as we decrease the temperature since in this case the interface thickness is significantly reduced even below 3–4 pixels which is the limit of stability of the derivative

discretizations. Note that there is a subtle difference when employing the vdW equation of state compared to the simplified equation of state used in the work of Lee and Fischer [52]. In the simplified equation of state the interface thickness is completely unrelated (uncoupled) to the equilibrium density ratio. This allows computations at very high density ratios while keeping the interface thickness to reasonable values (above 3–4 pixels). When a thermodynamic equation of state like the van der Waals or Carnahan-Starling is employed then there is a coupling between interface thickness and equilibrium density ratio through the thermodynamic theory of interfaces, causing additional challenges in the solution of the LBE models as T/T_c is further reduced.

C. Surface tension

The surface tension, γ, for a planar interface can be determined by the following formula [2,4,5,57]:

$$\gamma = \int_{-\infty}^{\infty} \kappa \left(\frac{d\rho}{dx}\right)^2 dx. \tag{45}$$

By defining

$$\gamma^* = \frac{b^2 \gamma}{(a\kappa)^{1/2}} \tag{46}$$

we have

$$\gamma^* = b^2 \left(\frac{\kappa}{a}\right)^{1/2} \int_{-\infty}^{\infty} \left(\frac{d\rho}{dx}\right)^2 dx. \tag{47}$$

By combining Eqs. (39) and (47) we take

$$\gamma^* = b^2 \left(\frac{\sigma}{\delta x}\right) \int_{-\infty}^{\infty} \left(\frac{d\rho}{d\tilde{x}}\right)^2 d\tilde{x} \tag{48}$$

or

$$\gamma^* = \gamma_0^* \left(\frac{\sigma}{\delta x}\right), \tag{49}$$

where $\tilde{x}=x/\delta x$, γ^* is a dimensionless surface tension following Bongiorno and Davis [5] with the additional use of Eq. (39) to relate parameters κ and a, and γ_0^* is in principle the value of the dimensionless surface tension when the pixel size is equal to the molecular diameter of the fluid.

Following the van der Waals theory for interfaces, it is straightforward to show that for the case of a planar interface, Eqs. (45) and (47) can be also written as

$$\gamma^* = \sqrt{2} \int_{\rho_g^*}^{\rho_l^*} [\Phi^*(\rho^*) - \Phi^*(\rho_l^*)]^{1/2} d\rho^*. \tag{50}$$

The latter equation has the advantage that it is independent of the density profile and thus it is not affected by issues of numerical differentiation, artificial interface thickness, etc.

Hence, we have calculated γ^* from Eq. (47) or (48) using the results of the LBM simulations, performed at a value of $\tilde{\kappa}=a$, for the two-distribution function models, and $\tilde{\kappa}=a/4$, for the single-distribution function models, and compared it with the respective results obtained from vdW theory using Eq. (50). The results for the two-distribution function Ψ_μ model are summarized in Table III, while those for the Lee-Fischer M model in Table IV. From these results it is evident that when γ^* is calculated using the uncorrected pixel sizes the relative error with respect to the analytic solution is quite significant even at $T/T_c=0.98$ (around 10%). On the other hand, when the corrected values for δx are used (see also Tables I and II) the respective LBE method gives an excellent prediction of the vdW surface tension with a relative error that is about 7% at $T/T_c=0.9$ dropping to less than 0.6% at $T/T_c=0.98$. Similar results have been found for the other two-distribution function LBE models as well as for the single-distribution Lee-Fischer C model. The surface tension predicted by the Lee-Fischer M model, on the other hand, is in excellent agreement with the exact results from the vdW theory even without a correction in the lattice spacing, δx.

TABLE III. Surface tensions for a planar interface using the Ψ_μ model.

	Ψ_μ model ($\tilde{\kappa}=a$)		Exact result (vdW theory)
T/T_c	γ^* uncorrected	γ^* corrected	γ^*
0.9009	1.66×10^{-2}	1.95×10^{-2}	1.82×10^{-2}
0.93	9.81×10^{-3}	1.12×10^{-2}	1.08×10^{-2}
0.95	5.94×10^{-3}	6.70×10^{-3}	6.57×10^{-3}
0.98	1.51×10^{-3}	1.68×10^{-3}	1.67×10^{-3}

D. Circular interface

As a final step we extend our analysis to circular interfaces. We have limited our calculations to two dimensions, in order to avoid excessive computations, although the extension to three dimensions is straightforward.

It is well known that in the absence of gravity, for a two-phase system, thermodynamics require that one phase should be a sphere (or circle in two dimensions) imbedded in the second phase [4]. Moreover, contrary to the case of the planar interface, κ is not the only parameter affecting the surface tension and the thermodynamics of the system, since the sphere radius, R, has also a very important role. The system

TABLE IV. Surface tensions for a planar interface using Lee-Fischer M model.

	Lee-Fischer M model ($\tilde{\kappa}=a/4$)		Exact result (vdW theory)
T/T_c	γ^* uncorrected	γ^* corrected	γ^*
0.9009	1.70×10^{-2}	1.95×10^{-2}	1.82×10^{-2}
0.93	1.03×10^{-3}	1.12×10^{-2}	1.08×10^{-2}
0.95	6.35×10^{-3}	6.66×10^{-3}	6.57×10^{-3}
0.98	1.65×10^{-3}	1.67×10^{-3}	1.67×10^{-3}

has a solution that is identical to that of the planar interface only when $R \to \infty$ [4]. As the drop, or bubble size decreases both liquid and gas densities increase above the respective planar interface values, according to Laplace's equation, which for the case of a circular drop gives the values of pressure inside and outside of the drop by the following expressions [52,58]:

$$p_l = p_l^{\text{sat}} + \frac{\rho_l^{\text{sat}}}{\rho_l^{\text{sat}} - \rho_g^{\text{sat}}}\left(\frac{\gamma}{R}\right), \tag{51a}$$

$$p_g = p_g^{\text{sat}} + \frac{\rho_g^{\text{sat}}}{\rho_l^{\text{sat}} - \rho_g^{\text{sat}}}\left(\frac{\gamma}{R}\right), \tag{51b}$$

where p_l and p_g are the pressures of the liquid and gas phases, respectively, γ is the interfacial tension and the superscript sat denotes bulk properties.

Once these pressure values are calculated the corresponding densities for the liquid and gas phase can be computed analytically through the use of the respective equation of state. Laplace's law becomes invalid, when $R \to 0$. It has been shown that the density in the neighborhood of $R=0$ (when the interface of the drop or bubble is very small) can be very different from the respective gas or liquid density values determined by the Maxwell construction curve [4].

Thus we proceed by performing simulations for static circular drops of different diameters, from 20 to 100 pixels, at $T/T_c=0.95$. We have chosen to work with the Ψ_μ model among the two-distribution function models, using $\tilde{\kappa}=a$ ($\delta x=\sigma$), since we have already shown for the case of a planar interface that at this value of $\tilde{\kappa}$ the bulk gas and liquid densities obtained from the simulations are identical to their respective thermodynamic values, while the corrected pixel size is $\delta x \sim 0.9\sigma$ at this temperature. On the other hand, we have also performed simulations with the single-distribution Lee-Fischer M model, using $\tilde{\kappa}=a/6.25$ ($\delta x=2.5\sigma$) for the same reasons as above while noting that at higher values of $\tilde{\kappa}$ the model becomes unstable. The radius of the drop is defined as the radius at which the density of the fluid is equal to the arithmetic mean of the center and bulk gas densities [62].

The results for the liquid and gas densities as functions of the drop radius, R, are presented in Figs 10 and 11. At large R, the densities are asymptotic to the respective values obtained for the case of a planar interface and are also very close to the thermodynamic values obtained by Maxwell's construction. As the drop size decreases both liquid and gas densities increase above the respective planar interface values. In all cases the predictions from both LBE models are in close agreement with each other and with the analytical solution obtained from Laplace's law. The maximum spurious velocity was of the order of 10^{-6} for the Ψ_μ model and of the order of 10^{-15} for the Lee-Fischer M model, in accord with previous studies [52]. Note that additional simulations with the other two-distribution function models and/or the Lee-Fischer C model, have shown almost identical quantitative behavior with the Ψ_μ model, in both densities and maximum spurious velocity values.

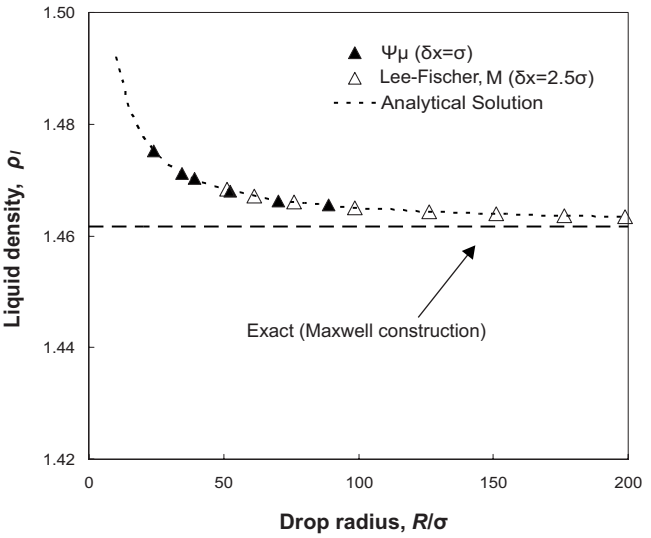

FIG. 10. Effect of drop radius R (in σ units) on liquid density ρ_l at the drop center using the Ψ_μ model ($\tilde{\kappa}=a$, $\delta x=\sigma$) and the Lee-Fischer M model ($\tilde{\kappa}=a/6.25$, $\delta x=2.5\sigma$) at $T/T_c=0.95$.

A final note must be made regarding the behavior of the systems at $\tilde{\kappa}=0$. In order to test the existence of artificial surface tension at $\tilde{\kappa}=0$ we performed additional simulations starting from a square drop at $t=0$. All three two-distribution function models as well as the Lee-Fischer C model, have converged into a circular drop after a large number of time steps, while in the Lee-Fischer M model, the initial square did not change its shape or size and remained as it was in the start of the simulation. This result indicates the existence of an artificial surface tension in all models except from the Lee-Fischer M model, which is the only one that does not employ central finite differences for the directional derivatives (note that schemes that implement mixed finite differences only for the directional derivatives have also preserved the original square shape of the drop).

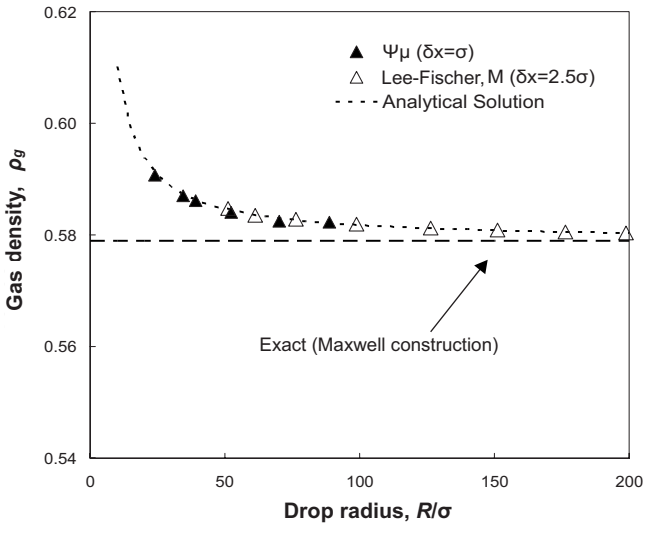

FIG. 11. Effect of drop radius R (in σ units) on bulk gas density ρ_g outside the drop using the Ψ_μ model ($\tilde{\kappa}=a$, $\delta x=\sigma$) and the Lee-Fischer M model ($\tilde{\kappa}=a/6.25$, $\delta x=2.5\sigma$) at $T/T_c=0.95$.

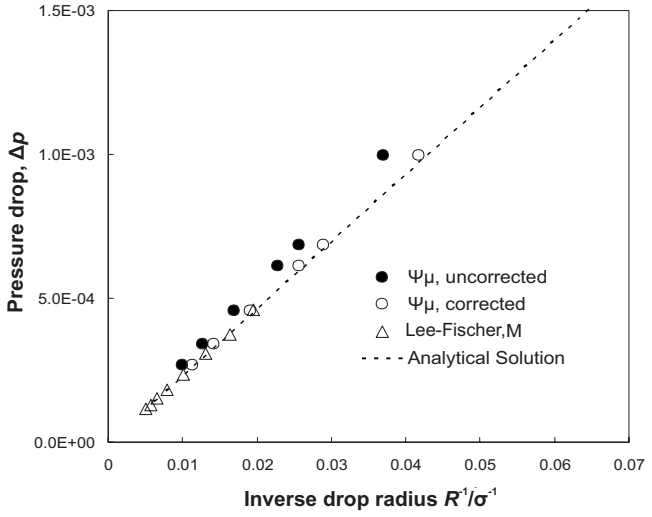

FIG. 12. Pressure drop Δp vs inverse drop radius $1/R$ (in σ^{-1} units) using the Ψ_μ model ($\tilde{\kappa}=a$, $\delta x=\sigma$) and the Lee-Fischer M model ($\tilde{\kappa}=a/6.25$, $\delta x=2.5\sigma$) at $T/T_c=0.95$.

E. Laplace's law and surface tension

It is well known that for the case of curved surfaces such as a spherical or cylindrical droplet, the Young-Laplace equation holds,

$$\Delta p = p_{\text{in}} - p_{\text{out}} = \frac{s\gamma}{R}, \tag{52}$$

where Δp is the pressure difference between the center of the drop and bulk of the surrounding gas phase, calculated from the respective density values through the respective equation of state and s is a numerical factor due to the curvature effects. It is straightforward to show that for spherical drops $s=2$, while for circular drops $s=1$. Following the definitions for the various dimensionless quantities it is straightforward to nondimensionalize Eq. (52) and obtain the following expression for the dimensionless surface tension γ^*:

$$\gamma^* = \frac{\Delta p R b^2}{a}, \tag{53}$$

where R is the drop radius in σ units.

In Fig. 12 we present a plot of Δp vs $1/R$ at $T/T_c=0.95$, for the two LBM models. In the same figure we have included the analytic solution based on Laplace's law and the exact results on the various thermodynamic properties from vdW theory on planar interfaces. It is seen that there is a perfect straight line fit, passing from the origin at least for $R>20\sigma$, where the simulations have been performed. Moreover, the Lee-Fischer M model, produces results that are in excellent agreement with the analytic solution, while the Ψ_μ model predictions are also in close agreement, provided that the necessary correction on the pixel size is done (i.e., $\delta x=0.89\sigma$ instead of $\delta x=\sigma$ for $\tilde{\kappa}=a$ and $T/T_c=0.95$). The surface tension is calculated from the slope of each line resulting in $\gamma^*=6.7\times10^{-3}$ for the corrected Ψ_μ model and $\gamma^*=6.5\times10^{-3}$ for the Lee-Fischer M model, which are both in excellent agreement with the respective value, obtained from vdW theory ($\gamma^*=6.57\times10^{-3}$). Note that similar results are expected for the case of a spherical drop, since the curvature effects are similar. However, we have chosen not to work in three dimensions to avoid excessive computational demands without gaining any further significant scientific knowledge.

IV. CONCLUSIONS

In the present study we investigate the thermodynamic consistency of LBE models developed by the forcing method by examining different numerical treatments of the LB equation. More specifically we have examined the standard two-distribution LBE model of He *et al.* [43] and two variants of it that employ the Gibbs-Duhem equation. Furthermore, we have also examined two versions of a recently proposed single-distribution model of improved stability and accuracy [52]. The effect of the interfacial density gradient parameter, κ, that controls surface tension, is related explicitly with the fluid characteristics, including temperature, molecular diameter, and lattice spacing, through the employment of a proper intermolecular interaction potential. The models are first applied for the calculation of bulk thermodynamic properties such as liquid and gas densities, pressure and chemical potential at various temperatures. Regarding the two-distribution function models significant improvement in the quantitative prediction of these properties is achieved when employing the Gibbs-Duhem equation for the calculation of intermolecular forces in conjunction with proper selection of the interfacial parameter, κ. For the case of the single-distribution function models, the mixed model gives an excellent prediction, which is the best among all LBE models examined, while the central model gives almost identical results with its respective two-distribution function version. Furthermore, the models are employed for the calculation of interfacial properties of gas-liquid systems including interface thickness and surface tension for both planar and curved interfaces of different circular drop sizes at static conditions. A comprehensive analysis of the interfacial properties of a van der Waals fluid using the two-distribution function LBE models and the one one-distribution central model reveals the appearance of artificial surface tension when central finite difference schemes are used for the description of the directional derivatives. Accordingly, a proper treatment is proposed that ensures thermodynamically consistent interfacial properties in accord with van der Waals's theory. The one-distribution mixed model, on the other hand, shows almost no artificial surface tension indicating thermodynamic consistency in the framework of the present theory. The results show that the models can capture both qualitatively and quantitatively the interface properties in accord with vdW theory, combining thermodynamic consistency and computational versatility.

Obviously the models are not very accurate when compared to real systems, but this is due to the inaccuracy of the physics of the vdW theory employed [5]. It is expected that the accuracy of models can be further improved by adopting the relevant ramifications of the vdW theory [5]. Moreover, LBM simulations under dynamic (flow) conditions with or without the presence of solid surfaces and comparison with

relevant detailed and approximate theories, is the subject of on-going research and will be presented in a future presentation.

We conclude by noting that the examined LBE models are valid quantitatively only at pixel sizes of the order of a few molecular diameters (depending on the value of temperature and the type of discretization of the directional derivatives) in order to predict the bulk and interface thermodynamic properties correctly. This limits the applicability of the models to relatively small-scale systems, which are nevertheless much larger than the ones employed in relevant molecular dynamics simulations but still much smaller than typical scales employed at the process or field level, except for nanotechnology applications. The apparent problem can be "cured" up to a point given the ease of parallelization of LBM methods and the increasing improvement in computational power.

[1] R. Evans, Adv. Phys. **28**, 143 (1979).
[2] J. S. Rowlinson and B. Widom, *Molecular Theory of Capillarity* (Dover, New York, 2003).
[3] J. W. Cahn and J. E. Hilliard, J. Chem. Phys. **28**, 258 (1958).
[4] A. J. M. Yang, P. D. Fleming III, and J. H. Gibbs, J. Chem. Phys. **64**, 3732 (1976).
[5] V. Bongiorno and H. T. Davis, Phys. Rev. A **12**, 2213 (1975).
[6] S. Nordholm, J. Gibson, and M. A. Hooper, J. Stat. Phys. **28**, 391 (1982).
[7] R. R. Nourgaliev, T. N. Dinh, T. G. Theofanous, and D. Joseph, Int. J. Multiphase Flow **29**, 117 (2003).
[8] R. Benzi, S. Succi, and M. Vergassola, Phys. Rep. **222**, 145 (1992).
[9] S. Chen and G. Doolen, Annu. Rev. Fluid Mech. **30**, 329 (1998).
[10] S. Succi, I. V. Karlin, and H. Chen, Rev. Mod. Phys. **74**, 1203 (2002).
[11] M. R. Swift, W. R. Osborn, and J. M. Yeomans, Phys. Rev. Lett. **75**, 830 (1995).
[12] M. R. Swift, E. Orlandini, W. R. Osborn, and J. M. Yeomans, Phys. Rev. E **54**, 5041 (1996).
[13] D. J. Holdych, D. Rovas, J. G. Georgiadis, and R. O. Buckius, Int. J. Mod. Phys. C **9**, 1393 (1998).
[14] D. J. Holdych, J. G. Georgiadis, and R. O. Buckius, Phys. Fluids **13**, 817 (2001).
[15] R. R. Nourgaliev, T. N. Dinh, and B. R. Sehgal, Nucl. Eng. Des. **211**, 153 (2002).
[16] A. N. Kalarakis, V. N. Burganos, and A. C. Payatakes, Phys. Rev. E **65**, 056702 (2002).
[17] A. N. Kalarakis, V. N. Burganos, and A. C. Payatakes, Phys. Rev. E **67**, 016702 (2003).
[18] A. J. Briant, A. J. Wagner, and J. M. Yeomans, Phys. Rev. E **69**, 031602 (2004).
[19] T. Inamuro, T. Ogata, S. Tajima, and N. Konishi, J. Comput. Phys. **198**, 628 (2004).
[20] T. Inamuro and T. Ogata, Philos. Trans. R. Soc. London, Ser. A **362**, 1735 (2004).
[21] X. Shan and H. Chen, Phys. Rev. E **47**, 1815 (1993).
[22] X. Shan and H. Chen, Phys. Rev. E **49**, 2941 (1994).
[23] N. S. Martys and H. Chen, Phys. Rev. E **53**, 743 (1996).
[24] A. R. Imre and G. Hazi, Int. J. Mod. Phys. C **13**, 649 (2002).
[25] G. Mayer, G. Hazi, A. R. Imre, T. Kraska, and L. V. Yelash, Int. J. Mod. Phys. C **15**, 459 (2004).
[26] J. Zhang, B. Li, and D. Y. Kwok, Phys. Rev. E **69**, 032602 (2004).
[27] M. C. Sukop and D. Or, Phys. Rev. E **71**, 046703 (2005).
[28] R. S. Qin, Phys. Rev. E **73**, 066703 (2006).
[29] R. Benzi, L. Biferale, M. Sbragaglia, S. Succi, and F. Toschi, Phys. Rev. E **74**, 021509 (2006).
[30] P. Yuan and L. Schaefer, Phys. Fluids **18**, 042101 (2006).
[31] M. Sbragaglia, R. Benzi, L. Biferale, S. Succi, K. Sugiyama, and F. Toschi, Phys. Rev. E **75**, 026702 (2007).
[32] X. He and L.-S. Luo, Phys. Rev. E **56**, 6811 (1997).
[33] S. Ansumali and I. V. Karlin, Phys. Rev. Lett. **95**, 260605 (2005).
[34] X. He and G. D. Doolen, J. Stat. Phys. **107**, 309 (2002).
[35] N. S. Martys, Physica A **362**, 57 (2006).
[36] A. Xu, S. Succi, and B. M. Boghosian, Math. Comput. Simul. **72**, 71 (2006).
[37] S. Chapman and T. G. Cowling, *The Mathematical Theory of Non-Uniform Gases* (Cambridge University Press, Cambridge, 1970).
[38] X. He, X. Shan, and G. D. Doolen, Phys. Rev. E **57**, R13 (1998).
[39] L.-S. Luo, Phys. Rev. Lett. **81**, 1618 (1998).
[40] L.-S. Luo, Phys. Rev. E **62**, 4982 (2000).
[41] Y. Shi, T. S. Zhao, and Z. L. Guo, Phys. Rev. E **73**, 026704 (2006).
[42] P. L. Bhatnagar, E. Gross, and M. Krook, Phys. Rev. **94**, 511 (1954).
[43] X. He, S. Chen, and R. Zhang, J. Comput. Phys. **152**, 642 (1999).
[44] R. Zhang, X. He, and S. Chen, Comput. Phys. Commun. **129**, 121 (2000).
[45] Q. Chang and J. I. D. Alexander, J. Comput. Phys. **212**, 473 (2006).
[46] S. Teng, Y. Chen, and H. Ohashi, Int. J. Heat Fluid Flow **21**, 112 (2000).
[47] A. Christea and V. Sofonea, Int. J. Mod. Phys. C **14**, 1251 (2003).
[48] A. Cristea, Int. J. Mod. Phys. C **17**, 1191 (2006).
[49] A. Cristea, G. Gonnella, A. Lamura, and V. Sofonea, Math. Comput. Simul. **72**, 113 (2006).
[50] A. J. Wagner, Phys. Rev. E **74**, 056703 (2006).
[51] T. Lee and C.-L. Lin, J. Comput. Phys. **206**, 16 (2005).
[52] T. Lee and P. F. Fischer, Phys. Rev. E **74**, 046709 (2006).
[53] G. R. McNamara, A. L. Garcia, and B. J. Alder, J. Stat. Phys. **81**, 395 (1995).
[54] R. Mei and W. Shyy, J. Comput. Phys. **143**, 426 (1998).
[55] Z. Guo and T. S. Zhao, Phys. Rev. E **71**, 026701 (2005).
[56] C. J. Atkins, *Equilibrium Thermodynamics* (Cambridge University Press, Cambridge, 1983).

[57] B. F. McCoy and H. T. Davis, Phys. Rev. A **20**, 1201 (1979).
[58] D. Jamet, O. Lebaigue, N. Coutris, and J. M. Delhaye, J. Comput. Phys. **169**, 624 (2001).
[59] S. J. Hemingway, J. R. Henderson, and J. S. Rowlinson, Faraday Symp. Chem. Soc. **16**, 33 (1981).
[60] S. M. Thompson, K. E. Gubbins, J. P. R. B. Walton, R. A. R. Chantry, and J. S. Rowlinson, J. Chem. Phys. **81**, 530 (1984).
[61] J. Horbach and S. Succi, Phys. Rev. Lett. **96**, 224503 (2006).
[62] A. H. Falls, L. E. Scriven, and H. T. Davis, J. Chem. Phys. **75**, 3986 (1981).